J. Fluid Mech. (1970), *vol.* 41, *part* 3, *pp.* 531–544
Printed in Great Britain

An investigation of the stability of a magnetohydrodynamic shear layer

By D. G. MALCOLM

Department of Mechanical Engineering
University of Saskatchewan, Saskatoon, Canada

(Received 4 June 1969 and in revised form 15 September 1969)

This paper presents an experimental investigation of the conditions of instability and post-critical flow in an electrically driven shear layer which has been previously studied both theoretically and experimentally. The shear layer forms as a primarily azimuthal flow in an electrically conducting fluid between the edges of two parallel and coaxial circular electrodes, mounted in insulating planes, when a current is passed between them in the presence of a strong, axially applied magnetic field. The aximuthal velocity at any radial position in the layer is maximum near the electrode planes and decreases to zero at the centreplane between the electrodes. Radial and axial secondary velocity components apparently exist, though smaller in magnitude than the azimuthal velocity throughout most of the layer.

The experiments employ a miniature *hot-film sensor* as an instantaneous velocity indicator in mercury. The following experimental results are reported.

$$R_c = 2420, \quad 150 \leqslant M \leqslant 350,$$

$$R_c = 345M^{\frac{1}{2}}, \quad 350 \leqslant M \leqslant 650,$$

where R_c is the critical Reynolds number of the shear layer, based upon the maximum velocity in the layer and the layer thickness, and M is the Hartmann number based upon the distance from the electrodes to the centreplane. For values of M below about 300, oscillograms of the hot-film signal show that the layer goes unstable in a chaotic fashion. For $M \geqslant 300$, however, the instabilities grow to produce a wave-like post-critical flow of steady amplitude. The waves are apparently parallel to the applied magnetic field and drift in the azimuthal direction at a constant proportion (10–15 %) of the critical velocity. The maximum intensity of the peak to peak fluctuations from the measured mean azimuthal velocity appears to be about 0·05. These fluctuations decrease to zero at the centreplane. By an approximate measurement of wavelength it is determined that the integral number of waves in the post-critical flow increases with M.

The physical mechanism governing the onset of instability has not been established. The manner in which hydrodynamic and electromagnetic forces interact with the destabilizing disturbances cannot be fully understood without further theoretical analysis.

1. Introduction

During the past decade many interesting theoretical studies have been published concerning the intense MHD free shear layers which form in certain configurations of duct flow, in flows around bodies and in electrically driven flows. The structure of a steady, electrically driven shear layer has been examined in detail experimentally by Hunt & Malcolm (1968) (H & M) and by Malcolm (1969*a*). The results of these experiments have been further discussed in the light of a rigorous theoretical analysis by Hunt & Stewartson (1969)

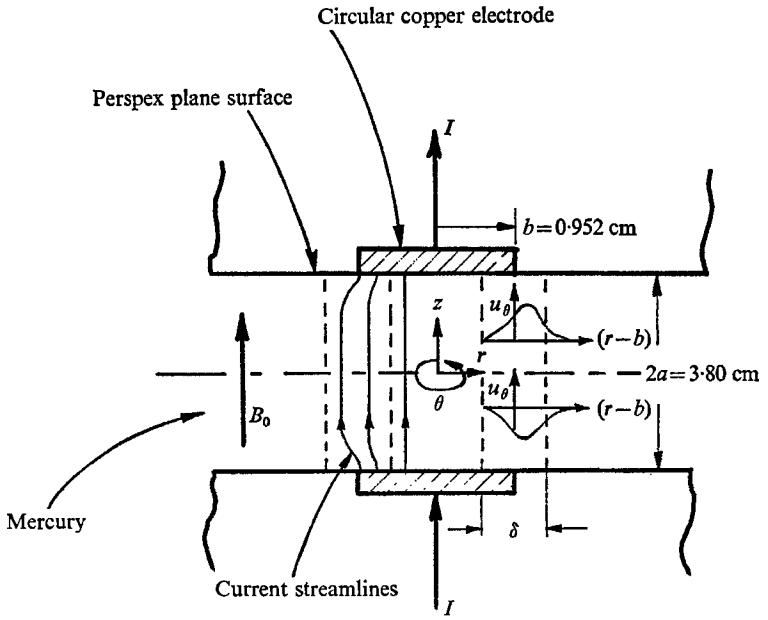

FIGURE 1. Top view of the apparatus and schematic current streamlines and velocity profiles in the electrically driven shear layer for $M \gg 1$.

(H & S). The present paper investigates experimentally the stability and post-critical flow of this same shear layer. It is hoped that the interesting results will point the way to a meaningful theoretical analysis of instability in this three-dimensional flow.

The electrically driven shear layer under consideration is formed as follows. When two circular electrodes at differing electric potentials are placed one in each of two parallel, insulating planes, between which is a fluid of electrical conductivity, σ, and viscosity, η, and when a strong, uniform magnetic field of intensity, B_0, is applied normal to these planes, an azimuthal flow is induced by electromagnetic forces in thin layers which join the edges of the electrodes as shown in the schematic top view of the apparatus in figure 1. The azimuthal flow is in opposite directions on either side of the centreplane.

The preliminary asymptotic analysis of H & M, valid for very high Hartmann number $M = B_0 a(\sigma/\eta)^{\frac{1}{2}}$, where $2a$ is the distance between the electrode planes, predicted that the azimuthal velocity at some radial position in the layer, $\rho = r/a$,

is maximum at a distance $O(aM^{-1})$ from the electrode and falls to zero at the centreplane. The thickness of the layers was predicted to be $\delta = O(aM^{-\frac{1}{2}})$. It was also shown that, providing $lM^{\frac{1}{2}} \gg 1$, where $l = b/a$ and b is the electrode radius, the non-dimensional velocity in the layer, $u_\theta M^{\frac{1}{2}} bl(\sigma\eta)^{\frac{1}{2}}/I$, where I is the total driving current, is a function of the non-dimensional distance from the edge of the electrode, $(\rho - l)\, M^{\frac{1}{2}}$, at any non-dimensional distance from the centreplane, $\zeta = \pm z/a$. The more rigorous study by H & S has since provided theoretical velocity profiles across the layer.

When M is large, there are two principal ways in which the H & S theory may become inadequate in a practical experiment using circular electrodes if the flow is driven hard by large currents. First, since the cylindrical shear layers are not uniform along their length, it cannot be expected that pressure gradients can just provide the centripetal accelerations and leave no radial flow. There must be a secondary circulation, which requires that the equations for the primary flow are modified by the inclusion of a Coriolis term. The relative importance of the latter increases as the flow is driven harder, but it is beyond the scope of the present paper to give even an order-of-magnitude basis for estimating the point at which the secondary flow begins to upset the primary. However, it is worth noting that the magnetic field not only affects the circulation because the thickness of shear layer and magnitude of azimuthal velocity depend on M, but also it directly inhibits the circulation, the vorticity of which is directed perpendicular to the direction of B_0. (For further discussion of the secondary flow see H & M and Malcolm (1969*a*).)

Figure 2 shows measured velocity profiles at various ζ for $M = 588$ using the hot-film technique. For comparison the results of Hunt & Stewartson (1969) are shown for $\zeta = 0{\cdot}905$. As discussed by Malcolm (1969*a*) the measured values are higher than the theoretical values, especially when $(\rho - l)\, M^{\frac{1}{2}} < 0$; this is believed to be caused by the radial pressure gradient, which is greatest near $\zeta = 1$ where u_θ is greatest, driving a large secondary flow and by the fact that the sensor is equally sensitive to radial and azimuthal velocities.† It was inferred by qualitative measurements that the secondary flow so driven finds its return path by circulating down through the shear layer and in towards the axis of symmetry near the centreplane. No such flow was observed at positions outside the fluid cylinder bounded by the shear layer.

The second way in which the H & S theory may become inadequate is that the flow reaches a state where it is unstable. Since $\partial/\partial r \gg \partial/\partial z$ in the layer, it might at first be supposed that the nature of the instability would not depend on there being variation in the z direction. The layer might become unstable somewhat in the manner of a two-dimensional plane jet. In the absence of a magnetic

† For the probe orientation used (see figure 3) the sensor is equally sensitive to radial and azimuthal velocity components. The short, cylindrical sensor (0·03 mm diameter and 0·5 mm sensitive length, approximately) is also quite sensitive to flow along its length so that z-wise components if present also have some effect on the observations. The maximum error in velocity measurement in addition to the directional effects is estimated to be $\pm 10\,\%$ of the maximum velocity measured in the layers (about 2·8 cm/sec). The details of the hot-film technique in low speed mercury flows and MHD measurement errors are discussed by Malcolm (1969*b*, *c*).

field the most unstable disturbances are then those whose wave-number vectors are parallel to the flow direction (see Squire 1933). Since in the present case the vorticity of such disturbances lies in the same direction as the magnetic field, electromagnetic forces have no influence (see Wooler 1961 and Hunt 1966). The

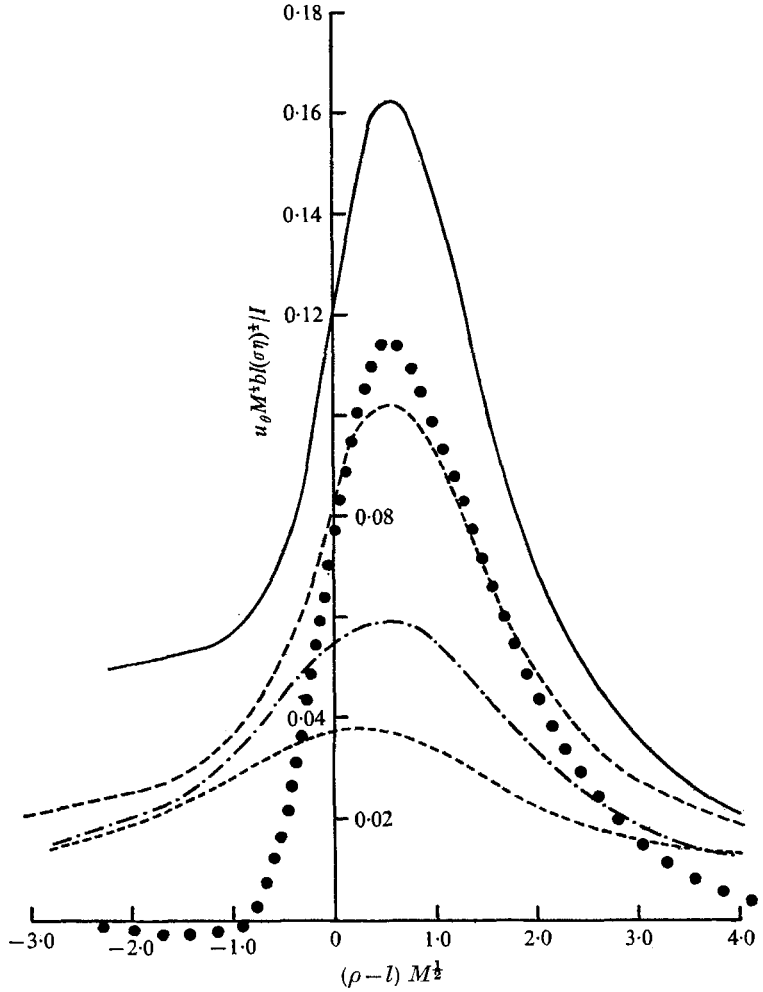

FIGURE 2. Radial profiles of azimuthal velocity for $M = 588$ at various distances from the centreplane: Hunt & Stewartson theory: ....., $\zeta = 0{\cdot}905$; experimental measurements: ———, $\zeta = 0{\cdot}905$; — — —, $\zeta = 0{\cdot}770$; — · —, $\zeta = 0{\cdot}522$; – – –, $\zeta = 0{\cdot}272$.

criterion for stability should then be that the Reynolds number R based on the thickness of, and the maximum velocity in, the layer is less than a critical value $R_c = R_c(M)$, but the dependence on M should not be strong since it only affects the situation through minor variations in the velocity profile of the layer.†

† In view of the cylindrical geometry, it might be conjectured that secondary-flow mechanisms could influence the stability. Although some large-scale secondary circulation as mentioned above, will always be present, the pattern might change to smaller-scale toroidal vortices similar to those formed between rotating cylinders (see Taylor 1923). No evidence was found in the present experiments of such a mode of instability, and it will

The present paper reports measurements of R_c ,and detailed investigation of the post-critical flow shows that for M sufficiently large it has a regular wave-like structure, which travels in the azimuthal flow direction. This suggests that the above analogy with a plane jet may indeed be fruitful, although a further complication arises from the fact that the 'waves' are found to have a regular phase relationship in the z direction. A mechanism must be found to feed energy from regions of high azimuthal velocity to regions of low velocity. Magnetohydrodynamic effects may here play a part.

2. Experiments and discussion

2.1. *Introduction*

The flow apparatus has been described in detail elsewhere (see H & M). Figure 1 contains the relevant dimensions, however. Figure 3 shows the orientation of the hot-film sensor (0·03 mm diameter and 0·5 mm sensitive length) in the flow. The

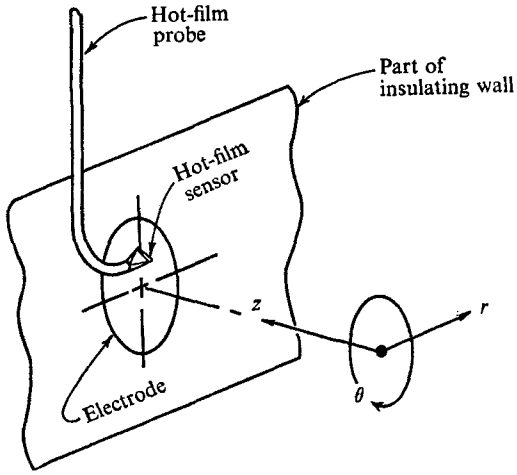

FIGURE 3. Horizontal orientation of the hot-film sensor in the apparatus.

probe could be traversed in a rectangular system of co-ordinates using a mechanism with three micrometer adjustments and could be positioned to within ± 0·001 in.

In order to study stability and the post-critical flow in the shear layer the driving current was increased while holding the magnetic field constant, for each of a large range of magnetic field values, until critical conditions were reached. The onset of instability was observed by positioning the hot-film sensor in the outer, low velocity region of the shear layer where it would not obstruct

not be considered further. It should, however, be mentioned that the experimental values of R_c for a given Hartmann number based on the layer thickness are only slightly smaller than the values of Reynolds number at which electrically driven flow between fixed cylinders becomes unstable for a given Hartmann number based on the gap width (see the experiments of Baylis (1964) in which an azimuthal flow is driven by radial currents interacting with an axial magnetic field).

the flow and following the anemometer output signal on the oscilloscope while the current was being increased. The accurate determination of critical conditions was facilitated by using an oscilloscope amplifier which contained the facility for filtering out all noise frequencies above 50 Hz while sensing frequencies as low as 0·06 Hz. The first sign of unsteadiness in the flow could thus be detected. The determination of a critical current was very tedious because of the necessity of approaching critical conditions very slowly and not forcing the onset of instability. When the current value was near critical it was necessary to observe the system for about 3 min before making the next very small increase. After reaching critical conditions, a return to stable flow could be effected by either increasing B_0 slightly at constant I or decreasing I slightly at constant B_0.

At the onset of instability, interesting phenomena observed on the oscilloscope were recorded using Polaroid film. From the information contained in these oscillograms at various probe positions, and from the measured values of I_c and M, it was possible to describe the phenomena involved in instability and the post-critical flow both qualitatively and quantitatively.

2.2. *Critical conditions in the flow*

Figures 4 and 5 show the I_c *vs.* M results, from which it appears that the data may be adequately described by the following empirical relationships:†

$$I_c = 2{\cdot}07M \times 10^{-3}, \quad 150 \leqslant M \leqslant 350, \tag{1}$$

and

$$I_c = 2{\cdot}95M^{\frac{4}{3}} \times 10^{-4}, \quad 350 \leqslant M \leqslant 650. \tag{2}$$

Critical Reynolds numbers may be approximately evaluated from the following definition of R_c, viz.

$$R_c = u_{\theta c}(6aM^{-\frac{1}{2}})\tilde{\rho}/\eta, \tag{3}$$

where $u_{\theta c}$ is the critical velocity which occurs near the electrode edge in the region of highest velocity and $6aM^{-\frac{1}{2}}$ is the approximate shear layer width as shown previously in the velocity profiles (e.g. see figure 2). Although it was not possible to come close enough to the wall to measure velocities in the region of highest velocity with the hot-film sensor, since that region occurs at a distance of approximately aM^{-1} away from the wall, use can be made of the theoretical prediction of H & S that the theoretical maximum velocity in the shear layer occurs near $\zeta = 1{\cdot}00$ and for very large M is given by:

$$u_\theta blM^{\frac{1}{2}}(\sigma\eta)^{\frac{1}{2}}/I = 0{\cdot}226.$$

From this information, and the fact that figure 2 showed reasonable agreement between theory and experiment, the critical velocity can be estimated as follows,

$$u_{\theta c} = \left(\frac{0{\cdot}226}{al^2\sigma^{\frac{1}{2}}\eta^{\frac{1}{2}}}\right)\frac{I_c}{M^{\frac{1}{2}}}. \tag{4}$$

† In appendix B of Hunt & Malcolm (1968) some preliminary hot-film results were given as

$$I_c \propto M, \quad M > 200.$$

The data plotted in figure 4 have been obtained in more carefully controlled experiments over a much wider range of M.

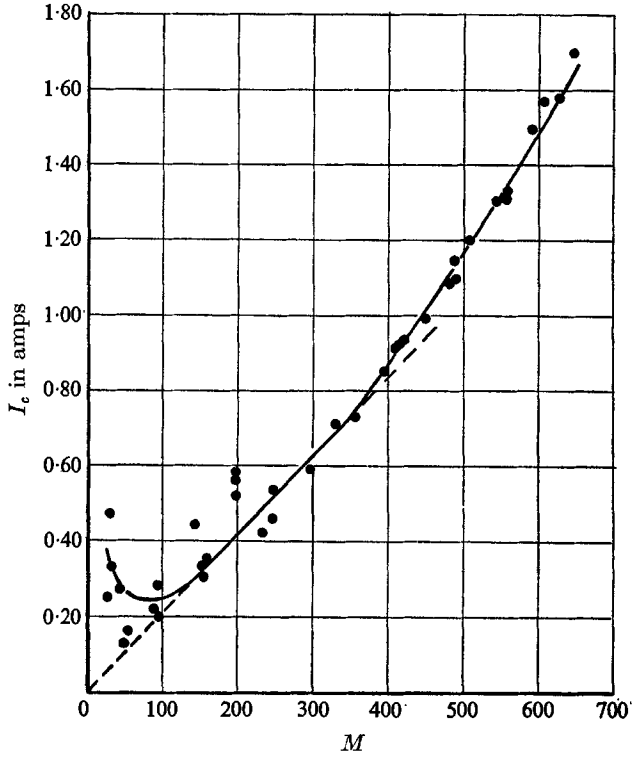

FIGURE 4. The dependence of critical driving current on Hartmann number in circular electrically driven flow, $l = 0{\cdot}502$.

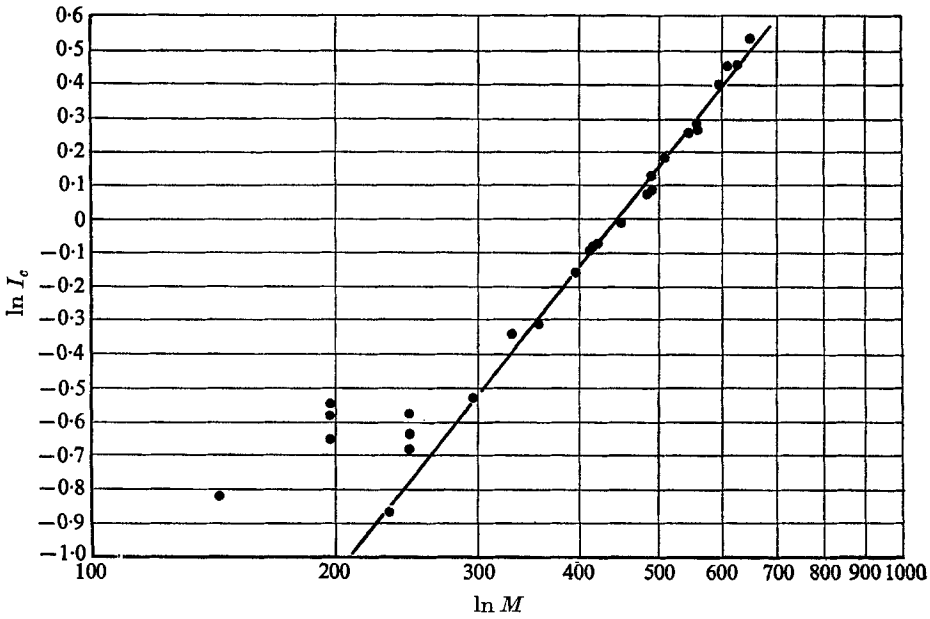

FIGURE 5. A plot of ln I_c *vs.* ln M.

Now, (4) can be substituted in (3) to give

$$R_c = \left(\frac{1{\cdot}36\tilde{\rho}}{l^2\sigma^{\frac{1}{2}}\eta^{\frac{3}{2}}}\right)\frac{I_c}{M}. \tag{5}$$

If I_c in (5) is replaced by (1) or (2) the critical Reynolds numbers can be calculated and are given as follows, using properties of mercury at 20 °C,

$$\left.\begin{aligned} R_c &= 2420, \quad 150 \leqslant M \leqslant 350, \\ R_c &= 345M^{\frac{1}{2}}, \quad 350 \leqslant M \leqslant 650. \end{aligned}\right\} \tag{6}$$

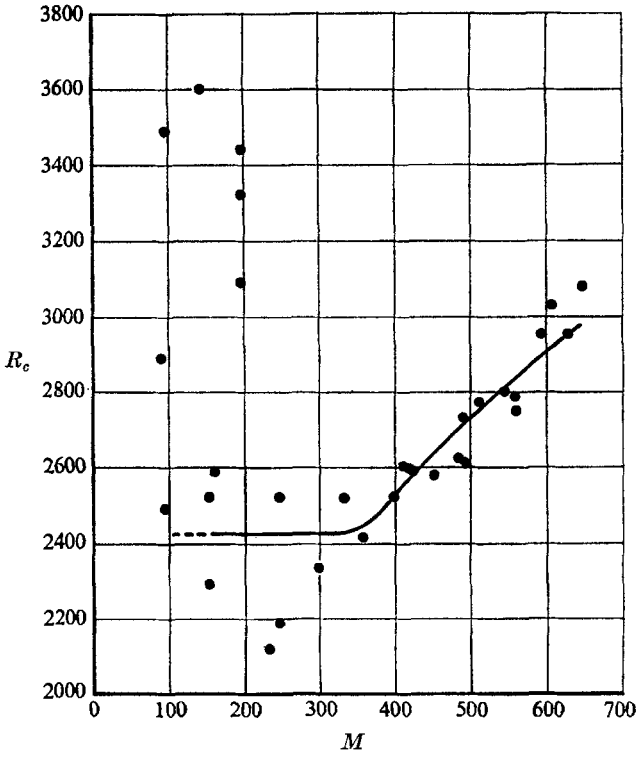

FIGURE 6. The dependence of R_c on M.

R_c is plotted against M in figure 6 along with the experimental data. In figures 4 and 6 it is observed that the experimental values of I_c and R_c become much more reproducible once M becomes large enough. As will be seen in the following oscillograms, the manner in which the shear layer goes unstable is not reproducible when M is less than 300, whereas when $M \geqslant 300$ instability always sets in in the same manner and ultimately produces a wave-like post-critical flow.

2.3. *Development of post-critical flow*

A predominant characteristic of the onset of instability for M lower than about 300 was the lack of reproducibility of the results under identical experimental conditions. For instance, figure 7 shows two separate runs at $M \simeq 150$. In

figure 7 (*a*), the flow became weakly turbulent following the onset of instability, whereas in figure 7 (*b*) the flow became oscillatory with a period of about 8 sec.

For values of $M \geqslant 300$ the destabilizing disturbances always developed gradually, without disrupting the main flow, into a non-axisymmetric flow having a wave-like form of steady amplitude, with a definite and reproducible

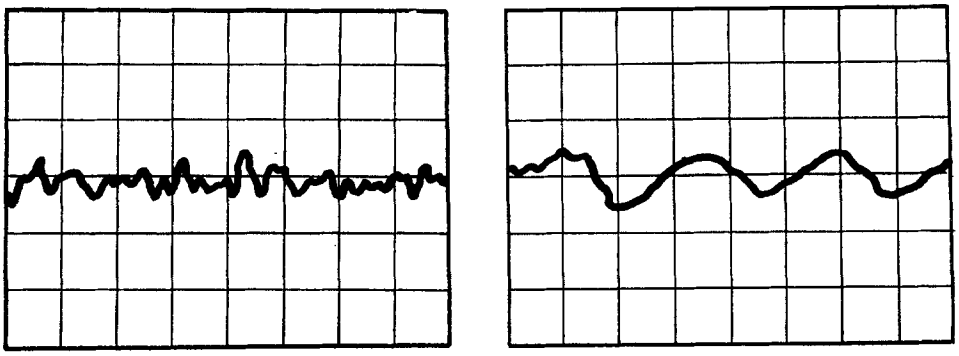

(*a*) (*b*)

FIGURE 7. Post-critical flow at critical conditions, (*a*) $M = 143$, $I_c = 0{\cdot}44$ amp, (*b*) $M = 153$, $I_c = 0{\cdot}30$ amp. *Scales:* 5 sec/division, 2 mV/division.

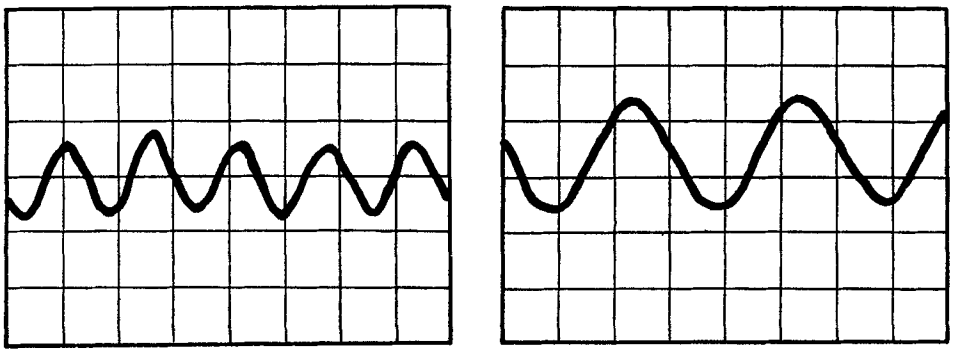

(*a*) (*b*)

FIGURE 8. Post-critical flow at critical conditions, (*a*) $M = 484$, $I_c = 1{\cdot}08$ amp (1 sec and 2 mV/division), (*b*) $M = 508$, $I_c = 1{\cdot}20$ amp (0·5 sec and 2 mV/division).

wave-number corresponding to each value of M. As an example of this predictable nature of the flow, figure 8 shows two separate observations at $M \simeq 500$. In these oscillograms the wave period is between 1·5 and 1·6 sec. For an example of a somewhat similar non-axisymmetric secondary flow which occurs in a rotating system of free hydrodynamic shear layers, see Hide & Titman (1967).

After examining the phenomena which occur at critical conditions, an attempt was made to find out the effect of a further increase in the driving current. These effects are illustrated in figures 9 and 10. Figure 9 (*a*) represents the case, $M = 485$, $I_c = 1{\cdot}08$ amp, when I is increased from I_c to 1·17 amp. The effect is to slightly increase the frequency of the initial oscillations and to introduce another mode of oscillation having a period about ten times as long as that of the initial one. This new mode may represent an 'out of balance' rotation of the whole cylindrical

flow system. When the current is further increased from 1·17 to 1·20 amps this new low frequency oscillation grows in amplitude until the situation in figure 9(*b*) is observed. The amplitude of the original higher frequency mode has now begun to oscillate as well. When the flow is pushed still faster by increasing I

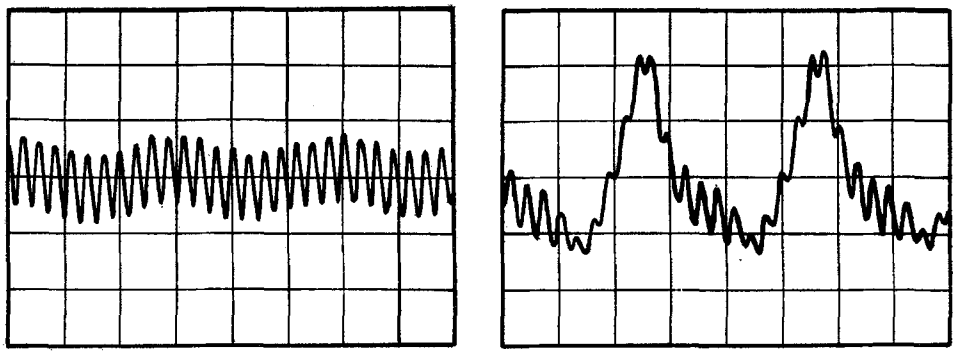

(*a*) (*b*)

FIGURE 9. Post-critical flow when $I > I_c$, $M = 484$. (*a*) $I = 1{\cdot}17$ amp. *Scales:* 5 sec/division, 5 mV/division. (*b*) $I = 1{\cdot}20$ amp. *Scales:* 5 sec/division, 10 mV/division.

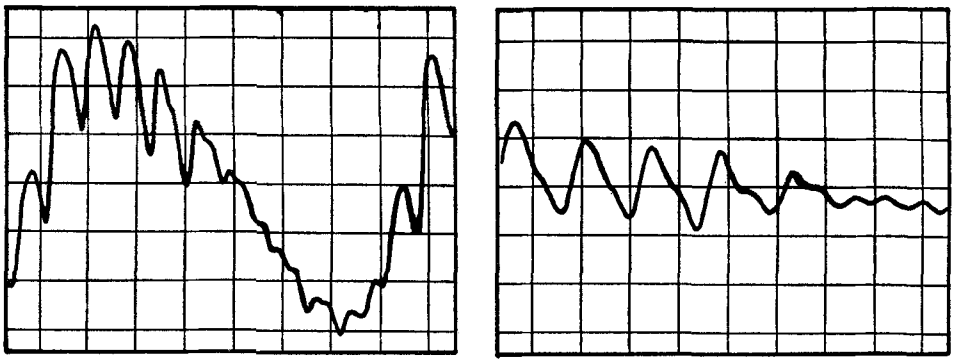

(*a*) (*b*)

FIGURE 10. Post-critical flow when $I > I_c$, $M = 490$, $I = 1{\cdot}30$ amp. (*a*) Using 0·06 Hz high pass filter. *Scales:* 2 sec/division, 10 mV/division. (*b*) Using 0·6 Hz high pass filter. *Scales:* 1 sec/division, 10 mV/division.

to 1·30 amp, the situation is somewhat similar to that in figure 9(*b*), and is shown in figure 10(*a*) and (*b*). The notable new change is the peculiar frequency doubling effect. Figure 10(*b*) shows this effect more clearly by filtering out the lowest frequency oscillation. It may be caused by the formation of waves of twice the original frequency, or by the beginnings of vortex formation behind the crests of the primary waves, as usually takes place when a hydrodynamic free shear layer goes unstable. At $M = 500$, the system could not be driven turbulent by increasing the current to as high as 2·00 amp, the limit of the constant current supply.

An experiment was designed to provide detailed information concerning the physical structure of the waves. In this experiment it was desired to determine, first, whether or not each of the waves was symmetrical about a line joining its

peak and the flow axis, secondly, whether or not the waves were aligned with B_0 and, finally, whether or not the waves were travelling in the flow direction and, if so, at what speed.

Figure 11 indicates that the waves are symmetrical. To obtain this information the hot-film sensor was first positioned in the outer portion of the shear layer at $\zeta = 0{\cdot}52$, $(\rho - l)\, M^{\frac{1}{2}} = 1{\cdot}97$ (in a flow characterized by $M = 607, I = 1{\cdot}60$ amp). Then the oscilloscope sweep rate was synchronized with the wave signal so that

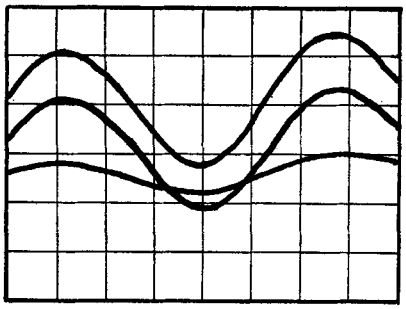

FIGURE 11. Evidence of wave symmetry.

the wave pattern was stationary on the screen. A photograph was taken, corresponding to one of the large amplitude signals in the figure. The sensor was then moved out in the radial direction from $(\rho - l)\, M^{\frac{1}{2}} = 1{\cdot}97$ to $(\rho - l)\, M^{\frac{1}{2}} = 2{\cdot}79$ where another exposure was taken, corresponding to the low amplitude signal in the figure. As a check on the synchronization of the wave pattern, the sensor was returned to its original position and a third exposure taken, corresponding to the other large amplitude trace in the figure. The lack of any discernible phase shift between the signals indicates that the waves were symmetrical.

Figure 12, plate 1, illustrates that the waves lie parallel to B_0. The corresponding flow conditions were, $M = 410, I = 0{\cdot}95$ amp. The sensor was positioned at $\zeta = 0{\cdot}50$, $(\rho - l)\, M^{\frac{1}{2}} = 2{\cdot}30$, and the sweep rate was again synchronized with the wave signal. The wave signal was photographed at constant radius at various stations in the z direction in the range $0{\cdot}50 \leqslant \zeta \leqslant 0{\cdot}90$. The lack of any discernible phase shift in the resulting oscillogram is convincing evidence that the waves were aligned with B_0.

In order to determine an approximate wave speed, a similar synchronization procedure was used, the results of which are observed in figure 13, plate 2. The sensor was positioned in a flow (described by $M = 509$, $I = 1{\cdot}24$ amp) at $(\rho - l)\, M^{\frac{1}{2}} = 2{\cdot}33$, directly above the z axis, and an exposure was taken, represented by one of the large amplitude traces which are superimposed in figure 13 (a). The sensor was then traversed in the horizontal plane (see figure 3) in the direction of u_θ, a distance of 0·125 in. where another exposure was taken. When referred to the cylindrical co-ordinate system this represents a movement out in the r direction as well as in the θ direction so that the trace, as photographed in figure 13 (a), is of lower amplitude. The original position was then returned to for a check exposure, represented by the other of the large amplitude, superimposed traces in the figure. With this figure and figure 13 (b) to give an accurate

value of the actual wave period, it is a simple matter to calculate the lag time brought about by moving the sensor the given distance in the flow direction, and hence the corresponding wave speed. When referred to the edge of the electrode, i.e. $(\rho - l) M^{\frac{1}{2}} = 0$, this speed is about 0·74 cm/sec.

By using equation (4) it is calculated that the above wave speed is 10–15 % of the critical velocity. Throughout most of the system, then, the fluid particle velocity is greater than the wave velocity. At each value of ζ the velocity of the fluid particles relative to phase velocity of the wave is different.

From the above approximate wave speed it is possible to estimate the wave-number, which in this context will be taken to mean the actual number of waves, n, spaced around the shear layer,

$$\frac{1}{n} = \frac{t_w u_w}{2\pi b}, \tag{7}$$

where t_w is the wave period. For the case illustrated in figure 13 it appears that $n \simeq 5{\cdot}4$, i.e. n must be 5 or 6. The experimental error does not allow a more exact calculation of n.

A similar calculation for n, using experimental results at $M = 415$, showed that in this case also n must be either 5 or 6. Upon increasing M to 603 it was found that the corresponding n is now 7 or 8. It seems therefore that the wave-number is some function of M. Since the cylindrical geometry of the flow allows an integral wave-number only, each n must hold over a certain range of M. The fact that n must be constant over a range of M allows the interesting observation that u_w is a constant proportion of $u_{\theta c}$, i.e. $u_w \propto u_{\theta c}$, over this same range of M. To demonstrate, let it be assumed that, for each value of n,

$$u_w \propto u_{\theta c}. \tag{8}$$

From (4) and (2) it is observed that,

$$u_{\theta c} \propto \frac{I_c}{M^{\frac{1}{2}}} \propto M^{\frac{5}{6}}, \quad 350 \leqslant M \leqslant 650. \tag{9}$$

Now, combining (7) to (9), it is expected that,

$$\frac{1}{n} \propto t_w M^{\frac{5}{6}}. \tag{10}$$

The wave-numbers at two values of M can be compared directly from this relationship. Table 1 applies the data from various runs at critical conditions to (10) in order to test (8). The fact that $t_w M^{\frac{5}{6}}$ is constant, within 3 %, as M varies from 355 to 509 is convincing evidence that the assumption, $u_w \propto u_{\theta c}$, holds so that, for each n, u_w is apparently a constant proportion of $u_{\theta c}$. The relationship (10) does not likely hold exactly for two values of M when n is different for each because the proportionality constant may be influenced by wave drag, etc. The column of probable n's in the table has been filled in assuming that this proportionality constant is little influenced by such effects.

Finally, an attempt was made to determine the variation in the intensity of the velocity disturbance associated with the travelling wave by traversing across the shear layer at $M = 603$ under critical conditions for two values of ζ, 0·522

and 0·770. The maximum peak to peak fluctuations in the streamwise direction have been estimated. These occur near $(\rho - l)\, M^{\frac{1}{2}} = 1{\cdot}51$ (very near to the outer point of inflexion on the steady velocity profile). The intensity of these peak to peak fluctuations, $u'_\theta/\bar{u}_\theta$, is estimated to be about 0·05 at both values of ζ. From

Run	M	$M^{\frac{1}{2}}$	t_w sec	$t_w M^{\frac{1}{2}}$	From (10) n_i/n_2	From (7) n	Probable n
1	296	115	3·12	359	0·74	—	4–5
2	355	134	1·97	264	1·00	—	5–6
3	395	146	1·80	263	1·00	—	5–6
4	415	153	1·75	268	0·98	5–6	5–6
5	449	163	1·62	264	1·00	—	5–6
6	509	181	1·50	272	0·97	5–6	5–6
7	603	208	0·96	200	1·32	7–8	7–8
8	607	209	0·97	203	1·30	—	7–8

TABLE 1. Integral wave-number determinations in the post-critical flow

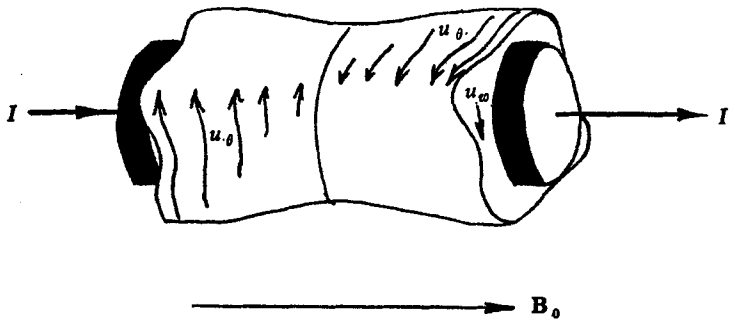

FIGURE 14. Sketch of probable wave-like post-critical electrically-driven flow.

this calculation, since u_θ falls as ζ decreases, it seems that the peak to peak fluctuations become less as ζ decreases. This is in qualitative agreement with the observation that both the fluctuations and the mean value of u_θ die out when the centreplane is reached, i.e. when $\zeta = 0$.

The situation is decidedly different to the similarly orientated MHD shear flow studied by Lehnert (1956), which was very nearly two-dimensional, in which the onset of instability was marked by the appearance of trains of vortices which were aligned with and unaffected by the magnetic field.

On the basis of the foregoing discussion, figure 14 shows a sketch of the distorted cylindrical flow system as it would conceivably appear in the mode of fully developed post-critical flow.

The interesting outcome of this study of the stability of a three-dimensional MHD free shear layer poses the question as to whether or not other similarly orientated shear layers, such as those occurring in the duct flows studied by Alty (1968), might behave similarly at the onset of instability. If the shear layers are very nearly two-dimensional, such as those studied experimentally by Lehnert (1956), it is unlikely that a similar post-critical flow will be observed. Further

analysis is necessary to establish the mechanism of instability in the cylindrical shear layer studied here. It may be that the growth of the disturbances is electromagnetically controlled, or that the growth is influenced by hydrodynamic forces peculiar to cylindrical flows.

I wish to thank Dr C. J. N. Alty at the University of Warwick, where the experiments were performed, Dr M. D. Cowley at the University of Cambridge for helpful discussions, and Mr A. E. Webb for assistance during the experiments. I also wish to thank the Royal Commission for the Exhibition of 1851 for support in the form of an Overseas Scholarship. The anemometry equipment was purchased through a grant from the Royal Society. I am grateful to Dr J. C. R. Hunt and Professor K. Stewartson for the use of their theoretical velocity profile in figure 2.

REFERENCES

ALTY, C. J. N. 1968 Submitted to *J. Fluid Mech.*
BAYLIS, J. A. 1964 *Nature*, **204**, 563.
HIDE, R. & TITMAN, C. W. 1967 *J. Fluid Mech.* **29**, 39.
HUNT, J. C. R. 1966 *Proc. Roy. Soc.* A **293**, 342.
HUNT, J. C. R. & MALCOLM, D. G. 1968 *J. Fluid Mech* **33**, 775.
HUNT, J. C. R. & STEWARTSON, K. 1969 *J. Fluid Mech.* **38**, 225.
LEHNERT, B. 1956 *Proc. Roy. Soc.* A **233**, 299.
MALCOLM, D. G. 1969*a* *Nature*, **224**, 909.
MALCOLM, D. G. 1969*b* *J. Fluid Mech.* **37**, 701.
MALCOLM, D. G. 1969*c* *DISA Information*, 9. (To be published.)
SQUIRE, H. B. 1933 *Proc. Roy. Soc.* A **142**, 621.
TAYLOR, G. I. 1923 *Phil. Trans. Roy. Soc.* A **223**, 289.
WOOLER, P. T. 1961 *Phys. Fluids*, **4**, 24.

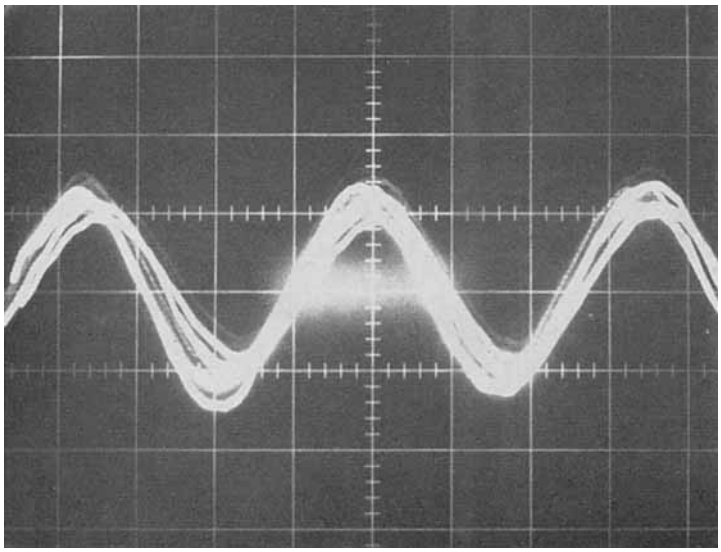

FIGURE 12. Evidence of alignment between the waves and the applied magnetic field.

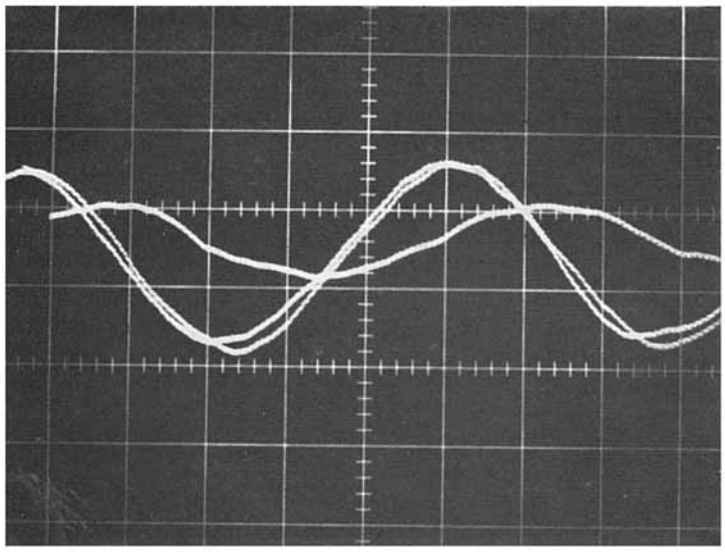

(*a*)

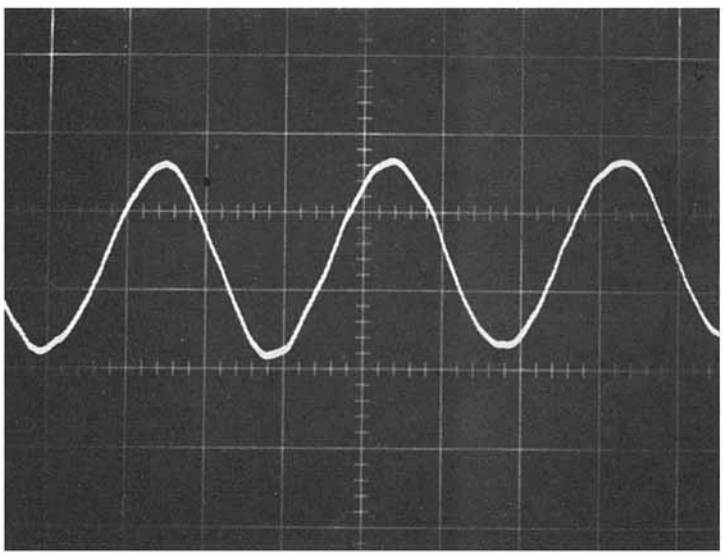

(*b*)

FIGURE 13. Determination of wave speed, (*a*) speed determination procedure using a synchronized sweep rate; (*b*) reference trace in real time: 0·5 sec/division.